Hindawi
Modelling and Simulation in Engineering
Volume 2017, Article ID 4938732, 11 pages
https://doi.org/10.1155/2017/4938732

Research Article

Systematic Theoretical Analysis of Dual-Parameters *RF* Readout by a Novel *LC*-Type Passive Sensor

Qiulin Tan,[1,2] Yanjie Guo,[1,2] Guozhu Wu,[1,2] Tao Luo,[1,2] Tanyong Wei,[1,2] Sanmin Shen,[1,2] Wendong Zhang,[1,2] and Jijun Xiong[1,2]

[1]*Key Laboratory of Instrumentation Science & Dynamic Measurement, Ministry of Education, North University of China, Taiyuan 030051, China*
[2]*Science and Technology on Electronic Test & Measurement Laboratory, North University of China, Taiyuan 030051, China*

Correspondence should be addressed to Qiulin Tan; tanqiulin@nuc.edu.cn

Received 9 November 2016; Revised 6 February 2017; Accepted 13 February 2017; Published 13 March 2017

Academic Editor: Aiguo Song

This paper systematically studied the simultaneous measurement of two parameters by a *LC*-type passive sensor from the theoretical perspective. Based on the lumped circuit model of the typical *LC*-type passive dual-parameter sensor system, the influencing factors of the signal strength of the sensor as well as the influencing factors of signal crosstalk were both analyzed. It is found that the influencing factors of the *RF* readout signal strength of the sensor are mainly quality factors (*Q* factors) of the *LC* tanks, coupling coefficients, and the resonant frequency interval of the two *LC* tanks. And the influencing factors of the signal crosstalk are mainly coupling coefficient between the sensor inductance coils and the resonant frequency interval of the two *LC* tanks. The specific influence behavior of corresponding influencing factors on the signal strength and crosstalk is illustrated by a series of curves from numerical results simulated by using MATLAB software. Additionally, a decoupling scheme for solving the crosstalk problem algorithmically was proposed and a corresponding function was derived out. Overall, the theoretical analysis conducted in this work can provide design guidelines for making the dual-parameter *LC*-type passive sensor useful in practical applications.

1. Introduction

Owing to their characteristics of wireless power supply and signal readout, various wireless passive sensors have been developed for harsh environments such as high-temperature [1–3] and in vivo environments [4, 5] in the past decade. However, most currently reported passive wireless sensors are single-parameter sensors, making it difficult for them to meet simultaneous multiparameter measurement requirements, such as pressure and temperature monitoring in turbine engines [6]. In addition, measuring multiple parameters by multiple single-parameter sensors will certainly deteriorate the installation adaptability and bring more intrusive interference. Therefore, developing micro passive sensors that can simultaneously measure multiple parameters has great significance for environmental monitoring in harsh environments.

Catering to the above-mentioned multiparameter measurement requirement, Zhang et al. proposed a concept of integrating two *LC* resonators into a single sensor to realize dual-parameters *RF* readout firstly (shown in Figure 1) [7]. Actually, the principle of this design was also used to enhance the signal strength of single-parameter passive sensors previously [8, 9]. Owing to the large overlapped area of the inductance coils of the sensor, its size does not increase significantly compared to the single-parameter counter-part. However, large overlapped area of inductances coils results in strong mutual coupling which make the crosstalk among multiple parameters nonignorable. Up to now, there is no scheme proposed to decouple the crosstalk. In order to avoid the crosstalk, Zhang et al. proposed a specific-winding inductance coils to suppress the mutual coupling between the sensor coils in their later paper [10], thus making the crosstalk negligible. Although the specific-winding method was quite successful in suppressing the crosstalk caused by the mutual inductance, this method makes the inductance of sensor coils decreased heavily, which in return shortens the readout

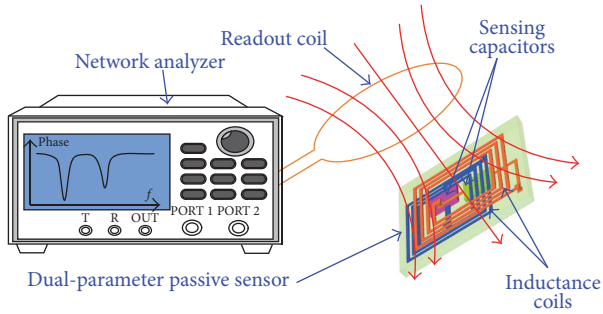

Figure 1: Schematic of dual-parameters *RF* readout by a *LC*-type passive sensor.

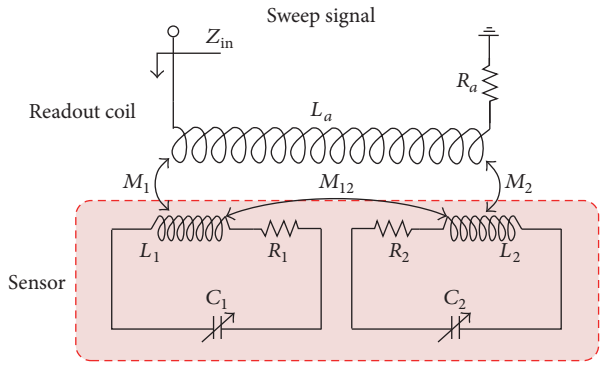

Figure 2: Lumped circuit model of the passive dual-parameter sensor system.

distance. The fact is that there is no paper systematically studied influencing factors of dual-parameters *RF* readout by the *LC*-type passive sensor, as well as the crosstalk decoupling scheme.

In order to provide guidelines for optimum design of the dual-parameter *LC*-type passive sensor system, problems of signal strength of the sensor and crosstalk between dip frequencies were chosen to be theoretically studied and discussed in this paper. More importantly, this paper proposed a decoupling function to solve the crosstalk problem successfully.

2. Analysis Model

Lumped circuit model of the *LC* type passive dual-parameter sensor system is illustrated in Figure 2, and the sensor is equivalent to two *LC* resonant circuits. L_1 and L_2 are the inductors of the sensor, R_1 and R_2 are the series resistances of the sensor, and C_1 and C_2 are the sensitive capacitors of the sensor. Similarly, the readout coil is equivalent to an inductor L_a and a series resistance R_a. In order to realize multiparameter measurement by a micro sensor with smallest volume, the inductance coils of the sensor usually have a large overlap area, which results in the existence of mutual inductance M_{12}. When the sensor was magnetically coupled with the readout coil, there are also mutual inductance M_1 and M_2, which corresponds to the coupling between the readout coil and the sensor inductors.

The input impedance of the readout coil can be given by [7]

$$\begin{aligned} Z_{\text{in}} &= R_a + j\omega L_a + j\omega M_{12}\frac{-\omega^2 M_2 M_{12} - j\omega M_1 Z_2}{Z_1 Z_2 + \omega^2 M_{12}^2} \\ &+ j\omega M_2\frac{-\omega^2 M_1 M_{12} - j\omega M_2 Z_1}{Z_1 Z_2 + \omega^2 M_{12}^2} = R_a + j\omega L_a \\ &+ j\omega k_1\sqrt{L_1 L_a} \\ &\cdot\frac{-\omega^2 k_2 k_{12} L_2\sqrt{L_a L_1} - j\omega k_1\sqrt{L_a L_1} Z_2}{Z_1 Z_2 + \omega^2 k_{12}^2 L_1 L_2} \\ &+ j\omega k_2\sqrt{L_2 L_a} \\ &\cdot\frac{-\omega^2 k_1 k_{12} L_1\sqrt{L_a L_2} - j\omega k_2\sqrt{L_a L_2} Z_1}{Z_1 Z_2 + \omega^2 k_{12}^2 L_1 L_2}, \end{aligned} \tag{1}$$

where ω is the angular frequency and is equal to $2\pi f$. And k_1 and k_2 are the coupling coefficients between the readout coil and the sensor coils. k_{12} are the coupling coefficients between the sensor coils. Z_1 and Z_2 are the equivalent impedance of these two *LC* tanks, respectively, and they can be given as

$$Z_1 = R_1 + j\omega L_1 + \frac{1}{j\omega C_1}, \tag{2a}$$

$$Z_2 = R_2 + j\omega L_2 + \frac{1}{j\omega C_2}. \tag{2b}$$

The resonance frequency of these *LC* tanks can be written as

$$f_1 = \frac{1}{2\pi\sqrt{L_1 C_1}}, \tag{3a}$$

$$f_2 = \frac{1}{2\pi\sqrt{L_2 C_2}}. \tag{3b}$$

Similar to the readout of the single-parameter *LC*-type passive sensor, it is theoretically feasible that the resonance frequencies change of the dual-parameter sensor can also be detected by measuring the impedance parameters (e.g., phase, real part, and magnitude) of the readout coil. In order to obtain unambiguous characteristic frequencies which can represent the resonant frequencies of two *LC* tanks of the sensor, it is necessary to make the resonant frequencies f_1 and f_2 separated within the measurement range of the sensor when we design the sensor. In this paper, the inductances L_1 and L_2 are designed to be constant and the resonant frequencies changes of the sensor depended on the change of capacitances C_1 and C_2.

Herein, by substituting the parameters in Table 1 into (1) and using MATLAB software for plotting curve, the frequency-phase curve illustrated in Figure 3 was obtained. It is clear that there are two obvious phase dips when the sensor magnetically coupled with the readout coil. However, the

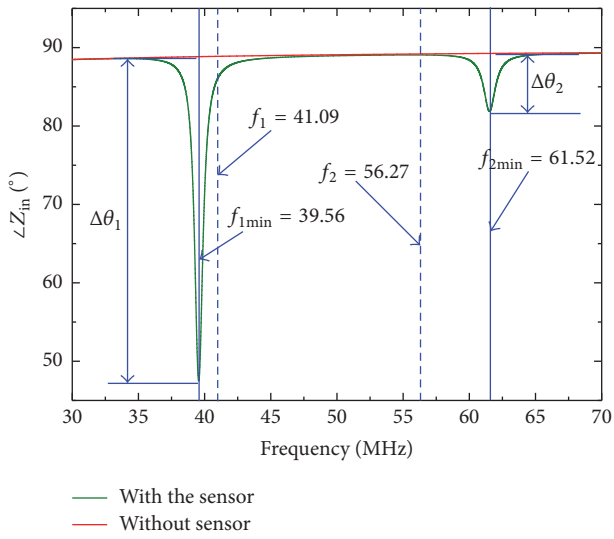

Figure 3: Phase versus frequency curve of the readout coil.

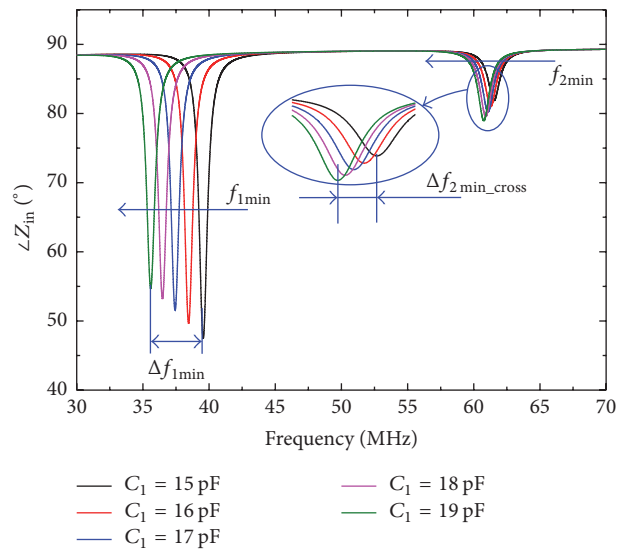

Figure 4: Schematic of the crosstalk of the dual-parameter passive sensor.

Table 1: Initial design parameters of the sensor system.

Symbol (unit)	Value
L_1, L_2, L_a (μH)	1
R_1, R_2, R_a (Ω)	5
C_1 (pF)	15
C_2 (pF)	8
k_1, k_2	0.1
k_{12}	0.3

phase dip frequencies (f_{1min} = 39.56 MHz, f_{2min} = 61.52 MHz in this design) are not equal to the resonant frequencies (f_1 = 41.09 MHz, f_2 = 56.27 MHz) of the sensor due to the mutual coupling k_{12}. Specifically, the mutual coupling between the sensor coils makes the phase dip frequencies apart compared to the resonant frequencies; that is, the dip frequency f_{1min} is smaller than the corresponding resonant frequency f_1 and f_{2min} is larger than f_2.

In spite of the inequality between dip frequencies and resonant frequencies, dual-parameter measurement by tracking the dip frequencies is absolutely feasible because the change of the resonant frequency will make the corresponding dip frequencies change. As shown in Figure 4, the dip frequency f_{1min} deceased monotonously when the capacitance C_1 increased from 15 pF to 19 pF (other parameters keep constant). It should be noted that the change of f_1 results in the drift of the dip frequency f_{2min}, and this phenomenon is a kind of crosstalk which is originally caused by the mutual coupling (k_{12}) between the sensor coils. The crosstalk strength can be indicated by the drift value Δf_{2min_cross}. Usually, the magnitude of the phase dip ($\Delta\theta_1$ and $\Delta\theta_2$ in Figure 2) should be large enough to make the readout of two phase dip frequencies possible within the measurement range.

3. Numerical Simulation and Analysis

3.1. Influencing Factors of the Sensor's Signal Strength. As illustrated in Figure 3, simultaneous dual-parameter measurement can be realized by tracking the dip frequencies f_{1min} and f_{2min}. Normally, passive sensors are developed for harsh-environment application, such as high-temperature and hermetic environment. And a typical situation is that the phase difference $\Delta\theta$ corresponding to the resonant point of a passive sensor will decrease at elevated temperatures due to the degraded Q factor of the LC resonator, which will make tracking the frequencies f_{1min} and f_{2min} harder, and will eventually make it impossible for the sensor to work in higher-temperature environment. Therefore, it is quite important to optimize the sensor system design to achieve large possible phase difference $\Delta\theta_1$ and $\Delta\theta_2$ if other conditions such as readout distance and sensor dimensions permit. In order to provide guidelines for optimizing the sensor system to achieve considerable readout signal strength, the influencing factors of $\Delta\theta_1$ and $\Delta\theta_2$ need to be analyzed.

3.1.1. Quality Factor. As for a LC resonator, its Q factor can be given as

$$Q = \frac{\omega_0 L_s}{R_s} = \frac{1}{2\pi R_s}\sqrt{\frac{L_s}{C_s}}. \quad (4)$$

It is obvious from (4) that the Q factor of the LC resonator mainly depends on its equivalent series resistance. Therefore, the resistance R_1 and resistance R_2 were changed to adjust the Q factors of the sensor in this part, and other parameters keep constant. As illustrated in Figure 5, the phase difference $\Delta\theta_1$ increased obviously with the increase of Q factor Q_1, and $\Delta\theta_2$ also showed a slight increase when Q_1 increased. It can be seen from Figure 6 that the increase of Q_2 resulted in an obvious increase of $\Delta\theta_2$ and a slight increase of $\Delta\theta_1$.

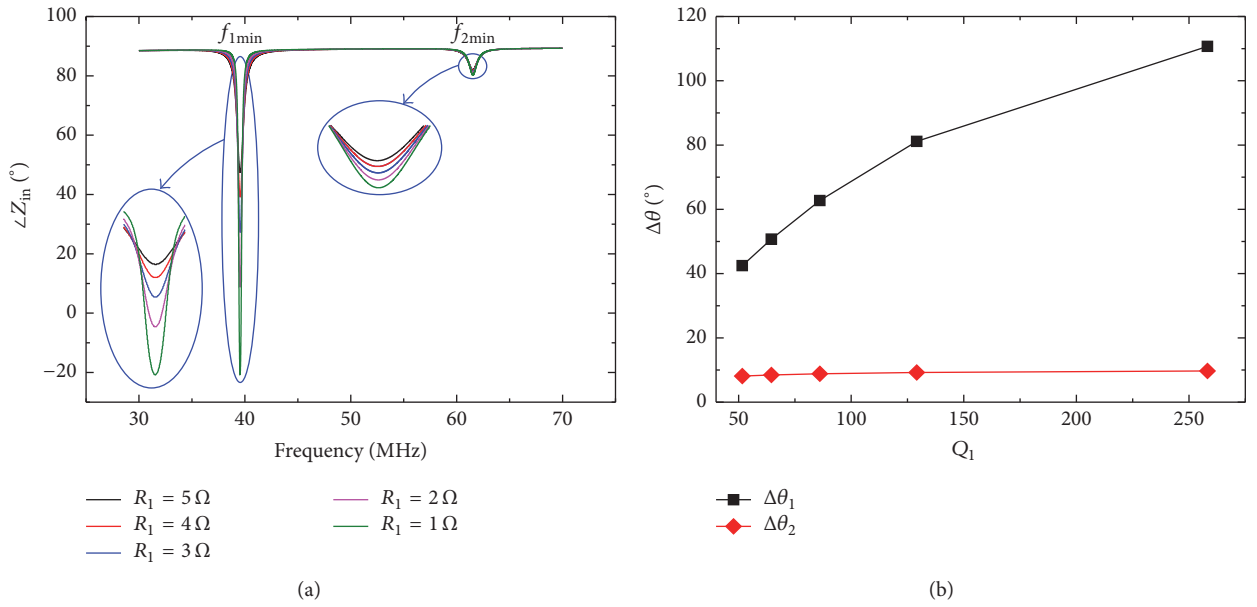

FIGURE 5: (a) Phase versus frequency curve of the readout coil when the Q factor Q_1 increased and (b) the influence of Q_1 on the value of $\Delta\theta_1$ and $\Delta\theta_2$.

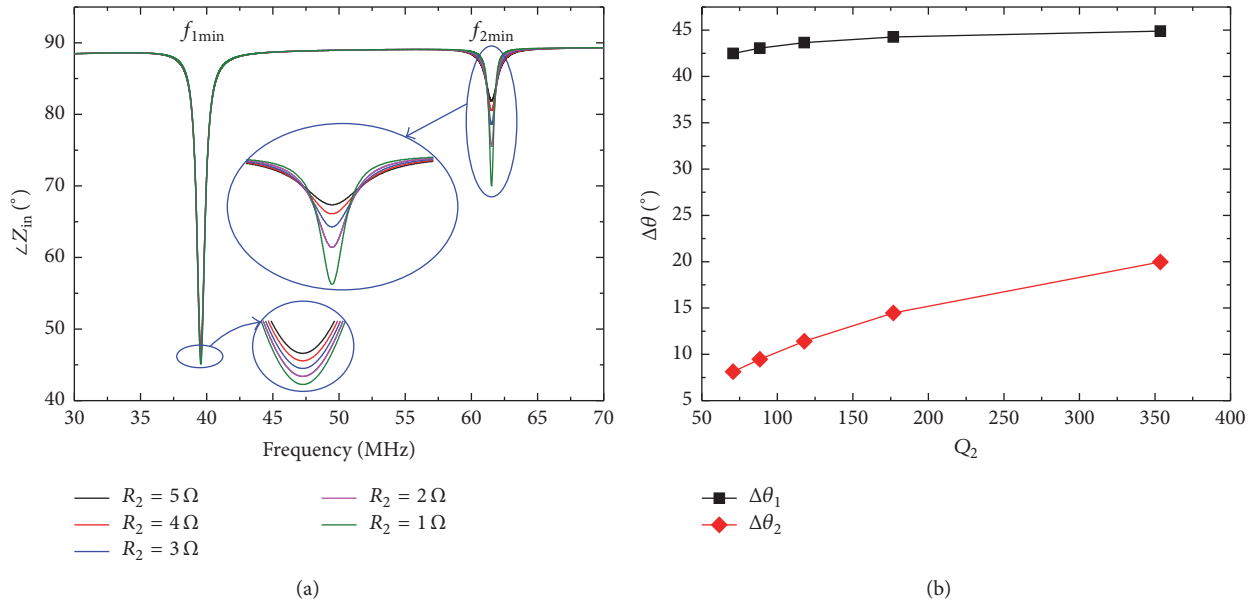

FIGURE 6: (a) Phase versus frequency curve of the readout coil when the Q factor Q_2 increased and (b) the influence of Q_2 on the value of $\Delta\theta_1$ and $\Delta\theta_2$.

Overall, it is sure that the increase of Q factor will make the corresponding phase difference increase significantly and make the other one increase slightly. So the Q factors of the LC resonators should be increased as much as possible by the optimum design to enhance the signal strength of sensor if other conditions permit.

3.1.2. Coupling Coefficients. In the dual-parameter passive sensor system, there are three coupling coefficients k_1, k_2, and k_{12}. As illustrated in Figure 7(a), the increase of k_{12} not only made the phase difference $\Delta\theta_1$ and $\Delta\theta_2$ and changed, but also made the obvious drift of f_{1min} and f_{2min}. Specifically, f_{1min} decreased and f_{2min} increased when k_{12} increased from 0.2 to 0.4 (other parameters keep constant). It can be seen from Figure 7(b) that the phase difference $\Delta\theta_1$ increased from 39.9° to 43.8° when k_{12} increased from 0.2 to 0.4, but $\Delta\theta_2$ decreased from 14.6° to 4.6°. Overall, increasing the coupling coefficient k_{12} makes phase difference corresponding to the

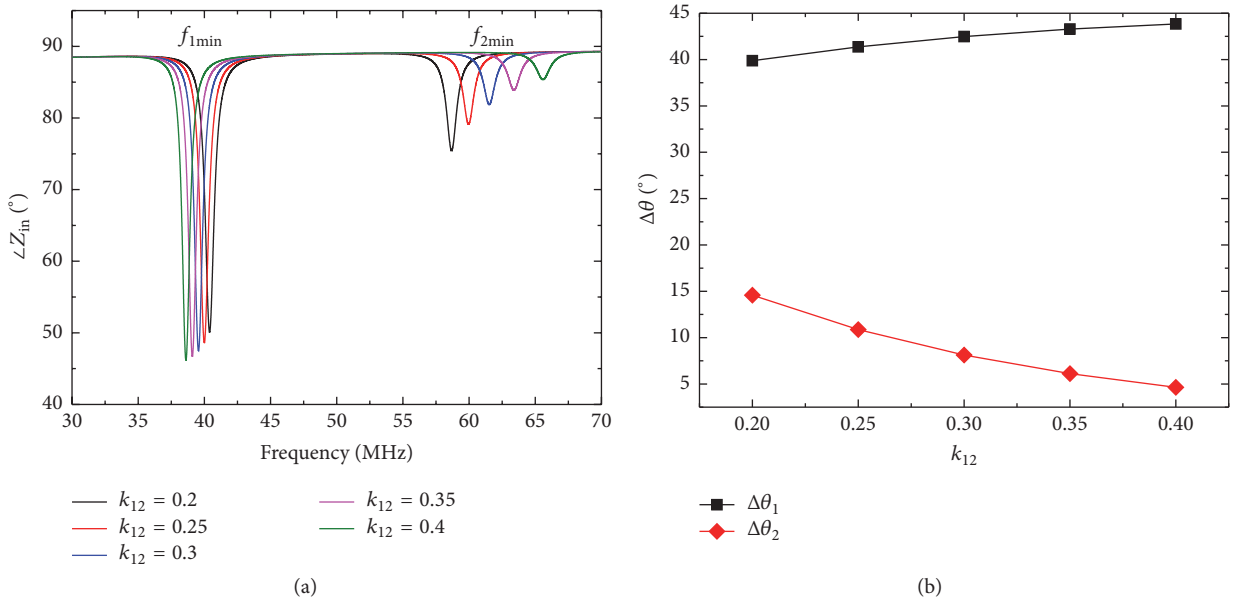

FIGURE 7: (a) Phase versus frequency curve of the readout coil when the coupling coefficients k_{12} increased and (b) the influence of k_{12} on the value of $\Delta\theta_1$ and $\Delta\theta_2$.

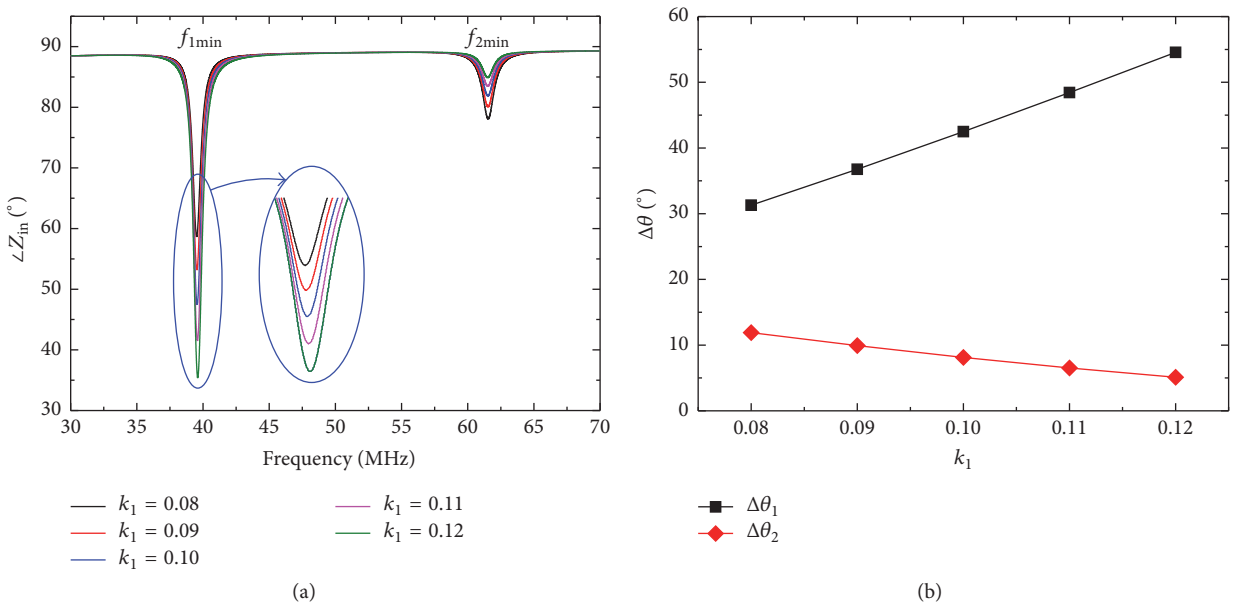

FIGURE 8: (a) Phase versus frequency curve of the readout coil when the coupling coefficients k_1 increased and (b) the influence of k_1 on the value of $\Delta\theta_1$ and $\Delta\theta_2$.

small frequency point f_{1min} increased slightly and makes the phase difference corresponding to f_{2min} decreased obviously. In the dual-parameter passive sensor system, the signal strength corresponding to the larger frequency f_{2min} was usually suppressed due to mutual coupling between the sensor coils. Therefore, considerable sensor strength can also be achieved by reducing k_{12}, which usually means to reduce the overlap area of the sensor coils in the sensor layout. However, many situations call for multiparameter sensor with volume as small as possible, which in return need the sensor coils overlapped as much as possible. So it is necessary to try to suppress the value of k_{12} if other restrictions permit.

It is obvious from Figure 8 that change of the coupling coefficient k_1 has significant influence on the value of $\Delta\theta_1$ and $\Delta\theta_2$. When k_1 increased from 0.08 to 0.12, $\Delta\theta_1$ increased from 31.3° to 54.6° and $\Delta\theta_2$ decreased from 11.9° to 5.1° accordingly. Therefore, the increase of the coupling coefficient corresponding to the small dip frequency f_{1min} will

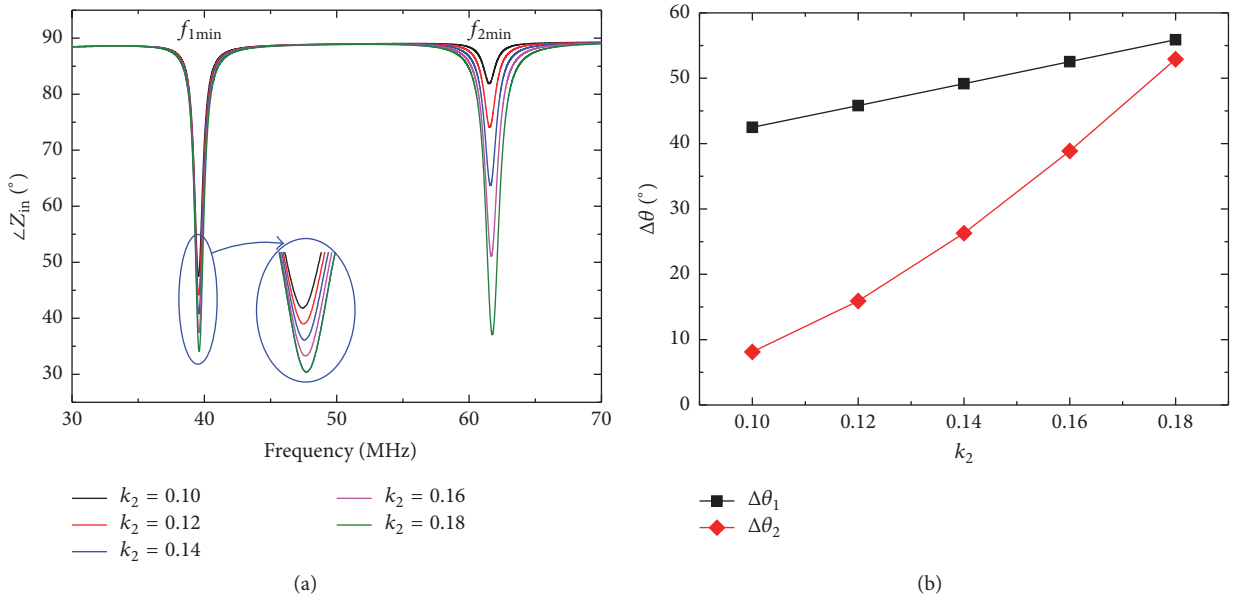

FIGURE 9: (a) Phase versus frequency curve of the readout coil when the coupling coefficients k_2 increased and (b) the influence of k_2 on the value of $\Delta\theta_1$ and $\Delta\theta_2$.

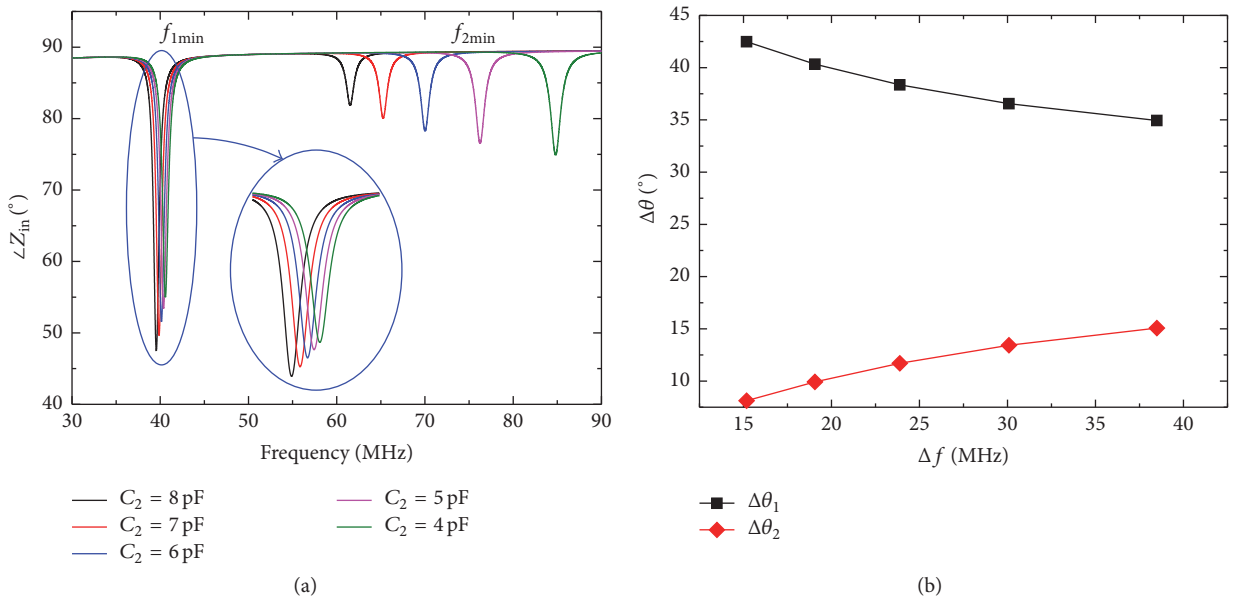

FIGURE 10: (a) Phase versus frequency curve of the readout coil when Δf increased and (b) the influence of Δf on the value of $\Delta\theta_1$ and $\Delta\theta_2$.

enhance the signal strength of f_{1min} and reduce the signal strength corresponding to the large dip frequency f_{2min}. Similarly, the influence of coupling coefficient k_2 on the signal strength of the sensor is illustrated in Figure 9. But unlike the influence of k_1, the increased k_2 not only enhances the signal strength of f_{2min} significantly but also makes $\Delta\theta_1$ increased obviously. It should be noted that the increase of k_1 and k_2 is usually based on the decrease of readout distance. Comprehensively analyzing the data illustrated in Figures 8(b) and 9(b), considerable signal strength of f_{1min} and f_{2min} can be achieved by properly reducing the value of k_1 without shortening the readout distance, that is, making k_1 less than the value of k_2.

3.1.3. Resonant Frequency Interval of the LC Tanks. The influence of resonant frequency interval Δf (equal to $f_2 - f_1$) on the sensor's signal strength is illustrated in Figure 10. It should be noted that the change of Δf was realized by changing the value of C_2, that is, by only changing the value of f_2. And the value of R_2 was changed accordingly to make the Q factor Q_2 keep constant. It is obvious that the influence of Δf on the value of $\Delta\theta_1$ and $\Delta\theta_2$ is similar to the

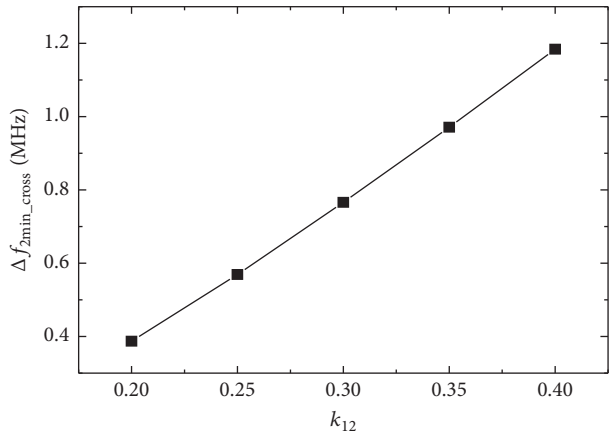

Figure 11: The influence of k_{12} on the value of $\Delta f_{2\min\_cross}$.

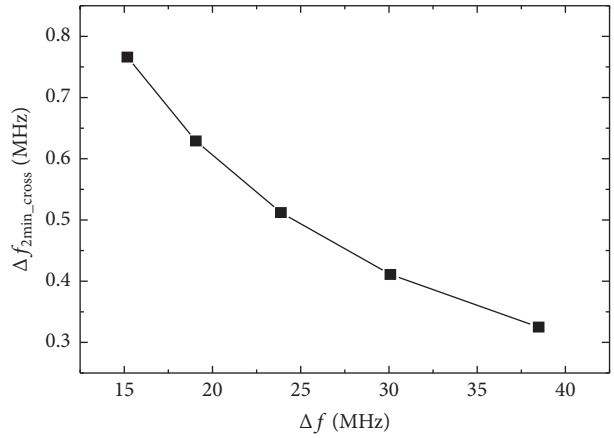

Figure 12: The influence of Δf on the value of $\Delta f_{2\min\_cross}$.

decrease of k_{12}. Therefore, broadening the resonant frequency interval Δf of the sensor can make the signal of f_2 strong and make $\Delta\theta_1$ decreased slightly. However, larger Δf means broader sweep bandwidth which will place greater demands on the readout circuit, that is, challenging the sampling speed and accuracy of the circuit. Overall, the resonant frequency interval Δf can be properly broadened to achieve better signal strength of the sensor without shortening the readout distance and increasing the sensor size, if the bandwidth, sampling speed, and accuracy of the readout circuit can fulfill the requirements.

3.2. Influencing Factors of the Signal Crosstalk. As illustrated in Figures 4 and 10, the value of $f_{1\min}$ not only depends on the corresponding resonant frequency f_1 when the coupling coefficients k_1, k_2, and k_{12} keep constant, but also depends on the resonant frequency of the other resonator (f_2), so does $f_{2\min}$. When the inductance $L_1 = L_2 = L$, the phase dip frequencies $f_{1\min}$ and $f_{2\min}$ can be derived as [7]

$$f_{\min}^2 = \frac{L(C_1+C_2) \pm \sqrt{L^2(C_1+C_2)^2 - 4C_1C_2L^2(1-k_{12}^2)}}{8\pi^2 C_1C_2L^2(1-k_{12}^2)}. \quad (5)$$

It can be seen from (5) that the values of $f_{1\min}$ and $f_{2\min}$ only depend on the coupling coefficient k_{12} and capacitances C_1 and C_2 if the inductances L_1 and L_2 keep constant. Actually, the value of C_1 and C_2 can also be expressed with above-mentioned resonant frequency interval Δf. If $k_{12} = 0$, (5) can be rewritten as

$$f_{1\min} = \frac{1}{2\pi\sqrt{LC_1}} = f_1, \quad (6a)$$

$$f_{2\min} = \frac{1}{2\pi\sqrt{LC_2}} = f_2. \quad (6b)$$

From (6a) and (6b), it can be seen that the fundamental reason for the crosstalk is the existence of mutual coupling between sensor coils. In this part, the influence of k_{12} and Δf on the crosstalk strength ($\Delta f_{2\min\_cross}$) was analyzed.

3.2.1. Coupling Coefficients. As illustrated in Figure 11, the crosstalk strength $\Delta f_{2\min\_cross}$ caused by the change of capacitance C_1 from 15 pF to 19 pF increased monotonously with the increase of k_{12}. Specifically, when k_{12} increased from 0.2 to 0.4, the crosstalk strength $\Delta f_{2\min\_cross}$ increased from 0.39 MHz to 1.18 MHz. Therefore, it can be concluded that reducing k_{12} can significantly reduce the crosstalk between two measurement parameters.

3.2.2. Resonant Frequency Interval of the LC Tanks. As illustrated in Figure 12, the crosstalk strength $\Delta f_{2\min\_cross}$ caused by the change of capacitance C_1 from 15 pF to 19 pF decreased monotonously with the increase of the resonant frequency interval Δf. Specifically, when Δf increased from 15.18 MHz to 38.48 MHz, the crosstalk strength $\Delta f_{2\min\_cross}$ decreased from 0.77 MHz to 0.33 MHz. Therefore, it can be concluded that properly increasing Δf can also reduce the crosstalk between two measurement parameters.

4. Crosstalk Decoupling

4.1. Decoupling Scheme. The requirement of miniaturization needs the sensor coils overlapped as much as possible, which makes the coupling coefficient k_{12} nonignorable, and it eventually makes the crosstalk nonignorable. Therefore, calibrating the sensor by directly using dip frequencies $f_{1\min}$ and $f_{2\min}$ will result in large measurement error. In order to avoid the error induced by the crosstalk, a decoupling scheme needs to be developed to realize accurate dual-parameter *RF* readout in the combinational environment. In this paper, a decoupling function as given in (7a) and (7b) will be developed to decouple the crosstalk algorithmically.

$$f_1 = F_1(f_{1\min}, f_{2\min}, k_{12}), \quad (7a)$$

$$f_2 = F_2(f_{1\min}, f_{2\min}, k_{12}). \quad (7b)$$

Equations (7a) and (7b) are the function which takes $f_{1\min}$, $f_{2\min}$, and k_{12} as the arguments and takes f_1 and f_2 as the dependent variables. The values of $f_{1\min}$ and $f_{2\min}$ can be readout by extracting the impedance of the readout coil,

and the values of k_{12} can be simulated by EM simulation software according to the layout of the sensor coils. Therefore, the resonant frequency of each LC tank can be achieved by substituting $f_{1\min}$, $f_{2\min}$, and k_{12} into the decoupling function.

4.2. Decoupling Function Derivation. The values of dip frequencies $f_{1\min}$ and $f_{2\min}$ can be derived from [7]

$$Z_1 Z_2 + \omega^2 M_{12}^2 = 0. \tag{8}$$

Equation (8) can be further rewritten as

$$\begin{aligned}
&\left[R_1 + j\omega L_1 + (j\omega C_1)^{-1}\right] \cdot \left[R_2 + j\omega L_2 + (j\omega C_2)^{-1}\right] \\
&\quad + \omega^2 k_{12}^2 L_1 L_2 = 0 \Longrightarrow \\
&R_1 R_2 + j\omega L_2 R_1 + \frac{R_1}{j\omega C_2} + j\omega L_1 R_2 - \omega^2 L_1 L_2 + \frac{L_1}{C_2} \\
&\quad + \frac{R_2}{j\omega C_1} + \frac{L_2}{C_1} - \frac{1}{\omega^2 C_1 C_2} + \omega^2 k_{12}^2 L_1 L_2 = 0 \Longrightarrow \\
&\underbrace{\left(\omega^2 k_{12}^2 L_1 L_2 - \omega^2 L_1 L_2 + R_1 R_2 + \frac{L_1}{C_2} + \frac{L_2}{C_1} - \frac{1}{\omega^2 C_1 C_2}\right)}_{\text{real part}} \\
&\quad + \left(j\omega L_2 R_1 + \frac{R_1}{j\omega C_{s2}} + j\omega L_1 R_2 + \frac{R_2}{j\omega C_{s1}}\right) = 0.
\end{aligned} \tag{9}$$

The left term of (9) is a complex number, and the sufficient and necessary condition for a complex number to be zero is that its real part and imaginary part should both be zero; that is,

$$\begin{aligned}
&\left(\omega^2 k_{12}^2 L_1 L_2 - \omega^2 L_1 L_2 + R_1 R_2 + \frac{L_1}{C_2} + \frac{L_2}{C_1}\right. \\
&\quad \left. - \frac{1}{\omega^2 C_1 C_2}\right) = 0.
\end{aligned} \tag{10}$$

Solving (10) to obtain the expression of dip frequency $f_{\min}$,

$$\begin{aligned}
\omega^2 = (2\pi f_{\min})^2 &= \frac{L_1 C_1 + L_2 C_2 + R_1 R_2 C_1 C_2}{2 L_1 L_2 C_1 C_2 (1 - k_{12}^2)} \\
&\pm \frac{\sqrt{(L_1 C_1 + L_2 C_2 + R_1 R_2 C_1 C_2)^2 - 4 L_1 L_2 C_1 C_2 (1 - k_{12}^2)}}{2 L_1 L_2 C_1 C_2 (1 - k_{12}^2)}.
\end{aligned} \tag{11}$$

The term $R_1 R_2 C_1 C_2$ can be omitted in (11) due to the fact that its order of magnitude is much less than that of the term $L_1 C_1 + L_2 C_2$. Therefore, (11) can be simplified as

$$\begin{aligned}
\omega^2 &= (2\pi f_{\min})^2 \\
&= \frac{L_1 C_1 + L_2 C_2 \pm \sqrt{(L_1 C_1 + L_2 C_2)^2 - 4 L_1 L_2 C_1 C_2 (1 - k_{12}^2)}}{2 L_1 L_2 C_1 C_2 (1 - k_{12}^2)}.
\end{aligned} \tag{12}$$

The dip frequencies $f_{1\min}$ and $f_{2\min}$ can be solved from (12) as

$$\begin{aligned}
f_{1\min} &= \sqrt{\frac{L_1 C_1 + L_2 C_2 + \sqrt{(L_1 C_1 + L_2 C_2)^2 - 4 L_1 L_2 C_1 C_2 (1 - k_{12}^2)}}{8\pi^2 L_1 L_2 C_1 C_2 (1 - k_{12}^2)}},
\end{aligned} \tag{13a}$$

$$\begin{aligned}
f_{2\min} &= \sqrt{\frac{L_1 C_1 + L_2 C_2 - \sqrt{(L_1 C_1 + L_2 C_2)^2 - 4 L_1 L_2 C_1 C_2 (1 - k_{12}^2)}}{8\pi^2 L_1 L_2 C_1 C_2 (1 - k_{12}^2)}}.
\end{aligned} \tag{13b}$$

By form variety of (3a) and (3b), it can be rewritten as

$$L_1 C_1 = \frac{1}{4\pi^2 f_1^2} = f_a, \tag{14a}$$

$$L_2 C_2 = \frac{1}{4\pi^2 f_2^2} = f_b. \tag{14b}$$

And substituting (14a) and (14b) into (13a) and (13b), (13a) and (13b) can be simplified as

$$f_{1\min} = \sqrt{\frac{f_a + f_b + \sqrt{(f_a + f_b)^2 - 4 f_a f_b (1 - k_{12}^2)}}{8\pi^2 f_a f_b (1 - k_{12}^2)}}, \tag{15a}$$

$$f_{2\min} = \sqrt{\frac{f_a + f_b - \sqrt{(f_a + f_b)^2 - 4 f_a f_b (1 - k_{12}^2)}}{8\pi^2 f_a f_b (1 - k_{12}^2)}}. \tag{15b}$$

By solving (15a) and (15b), the expression of f_a and f_b can be derived as

$$f_b = \frac{f_{1\min}^2 + f_{2\min}^2 + \sqrt{(f_{1\min}^2 + f_{2\min}^2)^2 - 4 f_{1\min}^2 \cdot f_{2\min}^2 \cdot (1/(1 - k_{12}^2))}}{8\pi^2 f_{1\min}^2 \cdot f_{2\min}^2}, \tag{16a}$$

$$f_a = \frac{f_{1\min}^2 + f_{2\min}^2 - \sqrt{(f_{1\min}^2 + f_{2\min}^2)^2 - 4 f_{1\min}^2 \cdot f_{2\min}^2 \cdot (1/(1 - k_{12}^2))}}{8\pi^2 f_{1\min}^2 \cdot f_{2\min}^2}. \tag{16b}$$

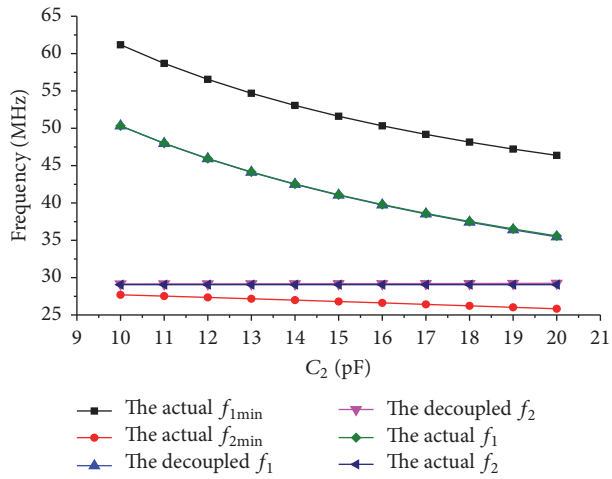

Figure 13: Decoupling theory validation of the algorithm.

Therefore, the decoupling function proposed in (7a) and (7b) can be rewritten as

$$f_1 = \frac{1}{2\pi \cdot \sqrt{f_a}}, \tag{17a}$$

$$f_2 = \frac{1}{2\pi \cdot \sqrt{f_b}}. \tag{17b}$$

5. Decoupling Method Validation

To verify the validity of multiparameter signal crosstalk decoupling algorithm shown in formulas (16a) and (16b), first the effectiveness of the decoupling algorithm is verified based on theoretical values simulation. As shown in Figure 13, the corresponding *LC* circuit resonance frequency of the sensor can be resolved by taking f_{1min} and f_{2min} and coupling coefficient ($k_{12} = 0.5$) into formulas (16a) and (16b). When one of the *LC* circuits of sensitive capacitance C_{s1} increases from 10 pf to 20 pf, only f_1 changes in theory, while the other *LC* circuit resonance frequency f_2 is changeless. As shown in Figure 13, by contrasting f_1, f_2 decoupled by f_{1min}, f_{2min}, k_{12} with actual f_1, f_2 in the same coordinate system, it is not difficult to find that the decoupled f_2 is greatly in accordance with the actual value, remaining almost unchanged, and the decoupled f_1 is as well in accordance with the actual f_1, presenting the same decreasing tendency. The decoupled resonant frequency is almost in accordance with the actual resonant frequency, but the decoupled f_2 slightly decreases with the decreasing of C_{s1}. It is mainly due to the omission of the inductance coil resistance in the derivation of decoupling algorithm.

By contrasting the experimental and decoupled data when k_{12} is 0.216 and 0.057 obtained by ADS simulation, respectively, it is seen that the decoupled f_T variation (74.8 kHz) is half small than when k_{12} is 0.057 (Figures 14 and 15). Of course, due to the omission of resistance in the derivation of decoupling algorithm, it cannot exclude the possibility for it causing decoupling precision which does not meet the actual test data of decoupling. Above all, further research needs to be conducted combining with experiments to improve the multiparameter signal crosstalk decoupling algorithm.

6. Conclusion

RF readout of dual-parameters by a novel *LC*-type passive sensor was theoretically analyzed. Confronting two critical problems in multiparameter *RF* readout, that is, problems of signal strength of the sensor and crosstalk between dip frequencies, this paper summarized the influencing factors of these two problems and characterized each factor's effect according to the numerical results based on calculating the analysis model of the sensor system. Last but not least, a decoupling function for solving the crosstalk problem was derived out. The study presented in this work provided theoretical design guidelines for the practical use of dual-parameter *LC*-type passive sensors.

Competing Interests

The authors declare no conflict of interests.

Authors' Contributions

All works with relation to this paper have been accomplished by all authors' efforts. The idea and design of the sensor were proposed by Qiulin Tan and YanJie Guo. The experiments of the sensor were completed with the help of Guozhu Wu and Tanyong Wei. Sanmin Shen and Tao Luo designed the fabrication method of the sensor. At last, every segment related to this paper is accomplished under the guidance of Jijun Xiong. Wendong Zhang has put forward valuable suggestions for the revision of the manuscript.

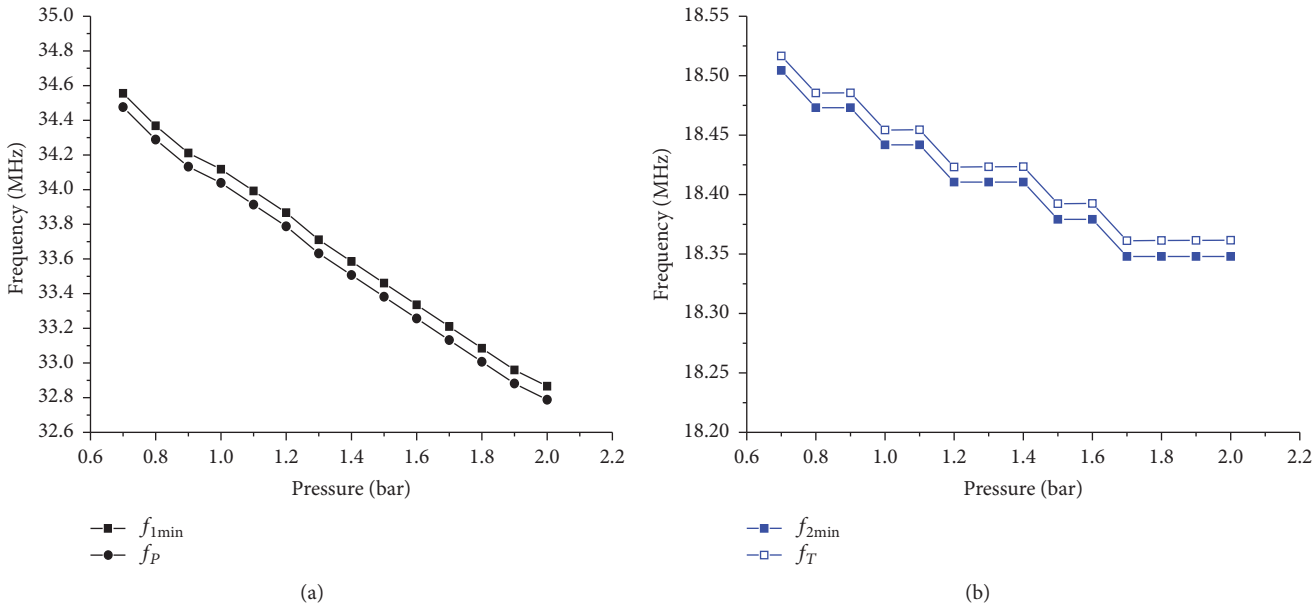

FIGURE 14: $k_{12} = 0.057$ decoupling results compared with the experimental data.

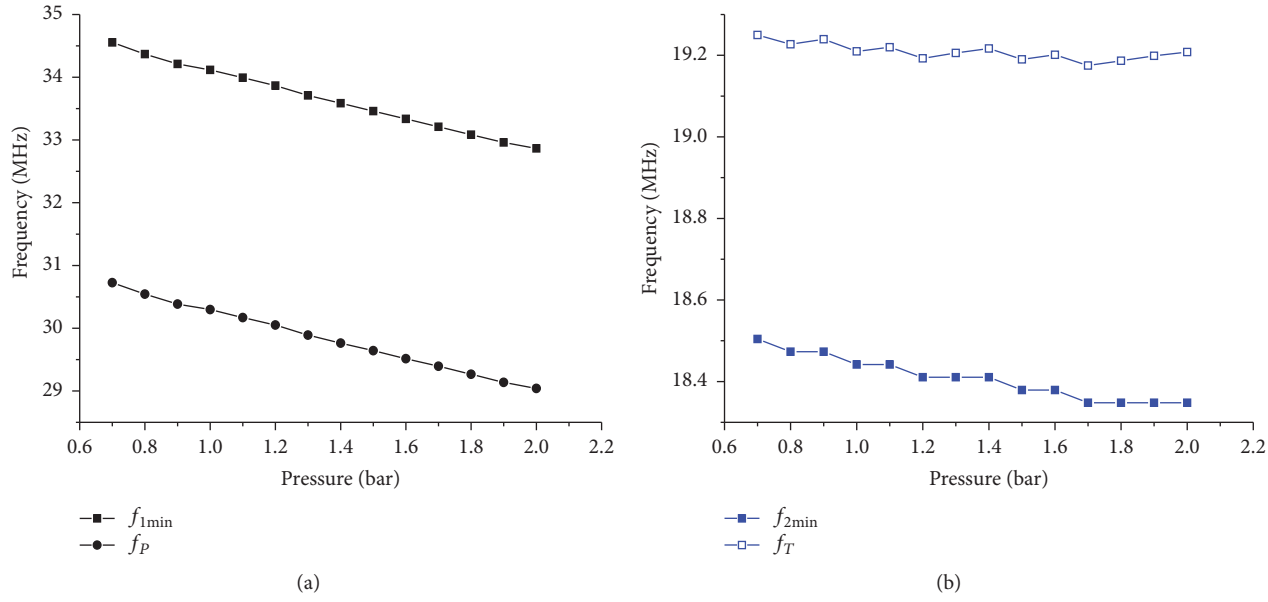

FIGURE 15: $k_{12} = 0.216$ decoupling results compared with the experimental data.

Acknowledgments

This work was supported by National Natural Science Foundation of China (Grant nos. 61471324 and 51425505) and the Outstanding Young Talents Support Plan of Shanxi Province.

References

[1] J. Xiong, Y. Li, Y. Hong et al., "Wireless LTCC-based capacitive pressure sensor for harsh environment," *Sensors and Actuators A: Physical*, vol. 197, pp. 30–37, 2013.

[2] M. A. Fonseca, *Polymer/ceramic wireless MEMS pressure sensors for harsh environments: high temperature and biomedical applications [Ph.D. thesis]*, 2007.

[3] G. J. Radosavljević, L. D. Živanov, W. Smetana, A. M. Marić, M. Unger, and L. F. Nađ, "A wireless embedded resonant pressure sensor fabricated in the standard LTCC technology," *IEEE Sensors Journal*, vol. 9, no. 12, pp. 1956–1962, 2009.

[4] P.-J. Chen, D. C. Rodger, S. Saati, M. S. Humayun, and Y.-C. Tai, "Microfabricated implantable parylene-based wireless passive intraocular pressure sensors," *Journal of Microelectromechanical Systems*, vol. 17, no. 6, pp. 1342–1351, 2008.

[5] P.-J. Chen, S. Saati, R. Varma, M. S. Humayun, and Y.-C. Tai, "Wireless intraocular pressure sensing using microfabricated minimally invasive flexible-coiled LC sensor implant," *Journal of Microelectromechanical Systems*, vol. 19, no. 4, pp. 721–734, 2010.

[6] W. C. Wilson and G. M. Atkinson, "Passive wireless sensor applications for NASA's extreme aeronautical environments," *IEEE Sensors Journal*, vol. 14, no. 11, pp. 3745–3753, 2014.

[7] C. Zhang, J.-Q. Huang, and Q.-A. Huang, "Design of LC-type passive wireless multi-parameter sensor," in *Proceedings of the 8th Annual IEEE International Conference on Nano/Micro Engineered and Molecular Systems (IEEE NEMS '13)*, pp. 256–259, April 2013.

[8] D. A. Sanz, C. Mitrosbaras, E. A. Unigarro, and F. Segura-Quijano, "Passive resonators for wireless passive sensor readout enhancement," *Applied Physics Letters*, vol. 103, no. 13, Article ID 133502, 2013.

[9] C. Zhang, L.-F. Wang, and Q.-A. Huang, "Extending the remote distance of LC passive wireless sensors via strongly coupled magnetic resonances," *Journal of Micromechanics and Microengineering*, vol. 24, no. 12, Article ID 125021, 2014.

[10] L. Dong, L.-F. Wang, and Q.-A. Huang, "Implementation of multi-parameter monitoring by an LC-type passive wireless sensor through specific-winding, stacked inductors," *IEEE Internet of Things Journal*, vol. 2, no. 2, pp. 168–174, 2015.